Weak palaeointensity results over a Pliocene volcanic sequence from Lesser Caucasus (Georgia): transitional record or time averaged field?

Elisa M. Sánchez-Moreno [1], Manuel Calvo-Rathert,[1,2] Avto Goguitchaichvili,[3] Lisa Tauxe,[4] George T. Vashakidze[5] and Vladimir A. Lebedev[6]

[1]*Departamento de Física, EPS Campus Rio Vena – Universidad de Burgos, Av. Cantabria, s/n, 09006 Burgos, Spain. E-mail: emsanchez@ubu.es*
[2]*Hawaii Institute of Geophysics and Planetology, School of Ocean and Earth Science and Technology, University of Hawaii at Manoa, Honolulu, HI 96822, USA*
[3]*Laboratorio Interinstitucional de Magnetismo Natural, Instituto de Geofísica Unidad Michoacán, UNAM – Campus Morelia, 58990 Morelia, México*
[4]*Scripps Institution of Oceanography, University of California - San Diego, La Jolla, CA 92093-0220, USA*
[5]*Alexandre Janelidze Institute of Geology – Ivane Javakhishvili Tbilisi State University, 1/9 M. Alexidze str., 0171 Tbilisi, Georgia*
[6]*Institute of Geology of Ore Deposits, Petrography, Mineralogy and Geochemistry – Russian Academy of Sciences (IGEM RAS), Staromonetny per., 35, 119017 Moscow, Russia*

SUMMARY

A palaeointensity study has been carried out on a Pliocene sequence of 20 consecutive lava flows where previous directional results seem to reflect anomalous behaviour of the Earth's magnetic field (EMF), which can be explained by a polarity transition record or non-averaged palaeosecular variation or both. Here, we perform a total of 55 palaeointensity determinations using the original Thellier–Thellier (TT) method and 100 with the IZZI method. We assess the performance of our selection criteria using a set of strict threshold values applied to a set of test data whose TRMs were acquired in known fields. Absolute palaeointensity determinations that passed our selection criteria were obtained on four specimens with the TT method and on 41 specimens with the IZZI method. Application of reliability criteria at a site level yielded palaeointensity results in 8 of 20 studied lava flows. We obtained median values of VADM between 28.9 and 45.6 ZAm^2 for the reverse polarity lower Apnia section, while the normal polarity upper section displayed a single value of 54.6 ZAm^2. The low palaeointensity values before a transitional direction lava flow and the higher value after it, suggest the common behaviour at the start of a polarity reversal and the recovery after it. However, an isolated record of a stable EMF, where the intensity is lower than the current for the same location (83.7 ZAm^2), cannot be discarded. Consequently, this interpretation would support a weak time-averaged field.

Key words: Palaeointensity; Magnetic field variations through time; Palaeomagnetism.

1 INTRODUCTION

The study of the Earth's magnetic field (EMF) characteristics and variations requires knowledge of both its direction and intensity. The direction of the ancient field can be measured directly because the magnetization recorded in a rock is usually parallel to the magnetizing field direction. Absolute palaeointensity cannot be measured directly as the magnetic remanence is only proportional, but not equal to the ancient field intensity. The combined (directional and intensity) analysis of palaeomagnetic results supplies new information for an enhanced understanding of the processes that occur in the outer core and control the geodynamo, the source of the fluctuations of the EMF (e.g. Barton 1982; Johnson & Constable 1996;

McElhinny *et al.* 1996; Merrill *et al.* 1996; Carlut *et al.* 1999; Merrill & Mcfadden 2003; Constable & Johnson 2005; Harrison 2007; Johnson *et al.* 2008; Glatzmaier & Coe 2015; Tarduno *et al.* 2015; Smirnov *et al.* 2017; Lund 2018).

Although so far several different palaeointensity determination methods have been used, those based on the original Thellier method (Thellier & Thellier 1959) are considered to be the most reliable ones, because they rely on a stringent physical basis. Nevertheless, absolute ancient field intensity data are scarcer than directional data, because they can only be obtained from materials in which the magnetization was acquired by a thermal mechanism, that is they have to carry a thermoremanent magnetization (TRM), as found in most volcanic rocks. In addition, in palaeointensity determinations,

in order to be successful, no magneto-chemical alteration of the remanence-carrying minerals may occur as a result of heating during the experiments, and the remanence should be ideally carried by single-domain grains (Thellier & Thellier 1959). The success rate in palaeointensity determinations is relatively low, and the currently available database shows a large degree of scatter—even for results from a single lava flow (e.g. Cromwell *et al.* 2015a).

Consecutive lava flow sequences provide a succession of instantaneous field states of the EMF at the time of emission as recorded by a TRM, thus allowing the analysis of both directional and intensity EMF variations. Regarding stable EMF periods, several palaeointensity studies performed during the last two decades have shown that average values of the virtual axial dipole moment (VADM) yield intensities of approximately half of the present-day value (current EMF strength ~80 ZAm^2, e.g. Juárez *et al.* 1998; Juárez & Tauxe 2000; Tauxe 2006; Lawrence *et al.* 2009; Tauxe *et al.* 2013; Cromwell *et al.* 2015b; Wang *et al.* 2015). Other studies, however, have yielded average VADM values during stable EMF periods which are near the present dipole moment (McFadden & McElhinny 1982; Heller *et al.* 2002; Smirnov & Tarduno 2003a, ; Tanaka *et al.* 1995; Valet *et al.* 2005). Knowledge about the characteristics of the EMF during anomalous periods like polarity reversals and geomagnetic excursions is even more limited, as the difficulty in finding records that cover the specific time period in which these events have occurred has limited the number of studies reported so far in comparison with those related to periods of a stable EMF (i.e. within normal or reverse polarity chrons).

This work focuses on the analysis of the palaeointensities recorded in the basaltic flow sequence of Apnia (Djavakheti Highland, Southern Georgia), which has been dated by the ^{40}K/^{40}Ar method (Lebedev *et al.* 2008) yielding an age between 3.70 and 3.09 Ma. The palaeomagnetic directions (Sánchez-Moreno *et al.* 2018) show, from bottom to top, 14 reverse polarity flows, followed by a transitional one and five normal polarity flows. Both mean poles of the normal and reverse populations disagree with the expected pole for the same age range. The virtual geomagnetic pole (VGP) scatter angle, with respect to the reference pole, in lower Apnia is 14.7°, matching the expected one (~15°–17° taken from Model G (McFadden *et al.* 1988) of palaeosecular variation of lavas (PSVL) fits to data from the last 5 Ma from McElhinny & McFadden (1997) and Johnson *et al.* (2008). Despite Model G having been reviewed and its limitations for accurately estimate the PSV latitudinal dependence having been pointed out (Doubrovine *et al.* 2019), it remains fully descriptive of the EMF behaviour during periods of stable polarity. Meanwhile in the upper sequence is VGP scatter yields a higher 21.3°, but its confidence interval spans the expected PSV scatter values. Directional results are inconsistent with stable EMF behaviour and could indicate a polarity transition or a record of several transitions, according to the ages obtained. On the other hand, the mismatch with the expected pole and the high dispersion could be the result of palaeosecular variation (PSV) that has not been averaged out. This second interpretation does not exclude the first one (Sanchez-Moreno *et al.* 2018). The palaeointensity data obtained from this work could provide new information to accept or reject the interpretation of a polarity reversal (or composite) record. Previous palaeomagnetic and palaeointensity results obtained on Plio-Pleistocene basaltic sequences in the volcanic region of Djavakheti display reliable records of both stable and unstable magnetic field regimes (Camps *et al.* 1996; Goguitchaichvili *et al.* 2000, 2001, 2009; Calvo-Rathert *et al.* 2011, 2013, 2015). Despite these previous studies, directional and especially reliable, high quality palaeointensity data in the Caucasus region are still scarce.

In this study, two different palaeointensity determination methods have been applied to the Apnia samples: The original Thellier method (TT, Thellier & Thellier 1959) and the IZZI method (Yu *et al.* 2004). As the aim of the study is obtaining reliable, high quality palaeointensity data, especially strict selection criteria for successful determinations have been applied. We have used the set of quality criteria proposed by Cromwell *et al.* (2015a), which was referred to as CCRIT by Tauxe *et al.* (2016), but we have divided the threshold values of the proposed criteria into two levels, with the goal of distinguishing two quality ranges. The first is called directly CCRIT, with threshold values similar to those of Tauxe *et al.* (2016). The second one, called RCRIT (Sánchez-Moreno 2018), is a somewhat less stricter version of the first one, although still stricter than other sets of criteria and threshold values frequently used (e.g. Kissel & Laj 2004; Leonhardt *et al.* 2004; Biggin *et al.* 2007; Tauxe *et al.* 2013).

2 GEOLOGICAL SETTING

The Apnia sequence (41°21′40″N, 43°16′02″E) was sampled in the volcanic Djavakheti Highland region, located in the central sector of the Lesser Caucasus (South Georgia, Fig. 1). This mountain range, included in the Alpine–Himalayan belt, is still being generated by the active collision of the Eurasian and Arabian plates. Within the so-called post-collision stage (late Miocene–Quaternary, Adamia *et al.* 2011) different phases of volcanic activity took place (Lebedev *et al.* 2008) in the Lesser Caucasus area: (I) Terminal Miocene (~7.5 Ma), (II) 3.7–1.8 Ma and (III) Last 800 ka. The volcanism, which generated the materials under study, corresponds to the second phase. A large number of volcanic cones and fissure volcanoes owing to NW–SE and NE–SW extensional strike-slip structures, which also developed by the compressional regime (Avagyan *et al.* 2010), characterize this phase. The numerous resulting consecutive basic lava flows created the current Djavakheti and Armenian plateaus. They are known as Akhalkalaki Formation in the Djavakheti region (Maisuradze & Kuloshvili 1999).

The Apnia sequence comprises 20 consecutive lava flows of calc-alkaline basalts and basaltic andesites, belonging to the Akhalkalaki Formation, that were sampled from top (AP01) to base (AP20). The thicknesses of the lava flows vary between 0.2 and 8 m, with a mode of 2 m (Fig. S1). Basic materials (basalts) have a rapid cooling rate, as compared to acidic lava flows, and in the Apnia sequence, we consider, that they can be estimated to lie within the order of days to weeks, or at most months for the most internal zones. Thus, cooling rates do not seem to vary significantly across the thickness range of studied flows (Fig. S1) and based on field observations we assume that flows are characterized by a similar rate of emplacement. The specimens measured in this study come from drilled cores on the outermost part of each lava flow. The sampled flows were sometimes altered by cracks and microfaults, and in certain spots were weathered or filled with material from the upper flow, forming veins and pseudo-dykes. Hence, extreme caution was taken during the palaeomagnetic sampling, to avoid the altered areas and to look for outcrops of the same lava flows without alteration.

The sequence was sampled with a portable water-cooled drill and the cores were directly oriented in the field with both solar and magnetic compass, and inclinometer. K–Ar ages ($\pm 2\sigma$) obtained in these flows yield ages of 3.09 ± 0.10 Ma for flow AP01, 3.28 ± 0.10 Ma for flow AP05, 3.75 ± 0.25 Ma for flow AP07 and
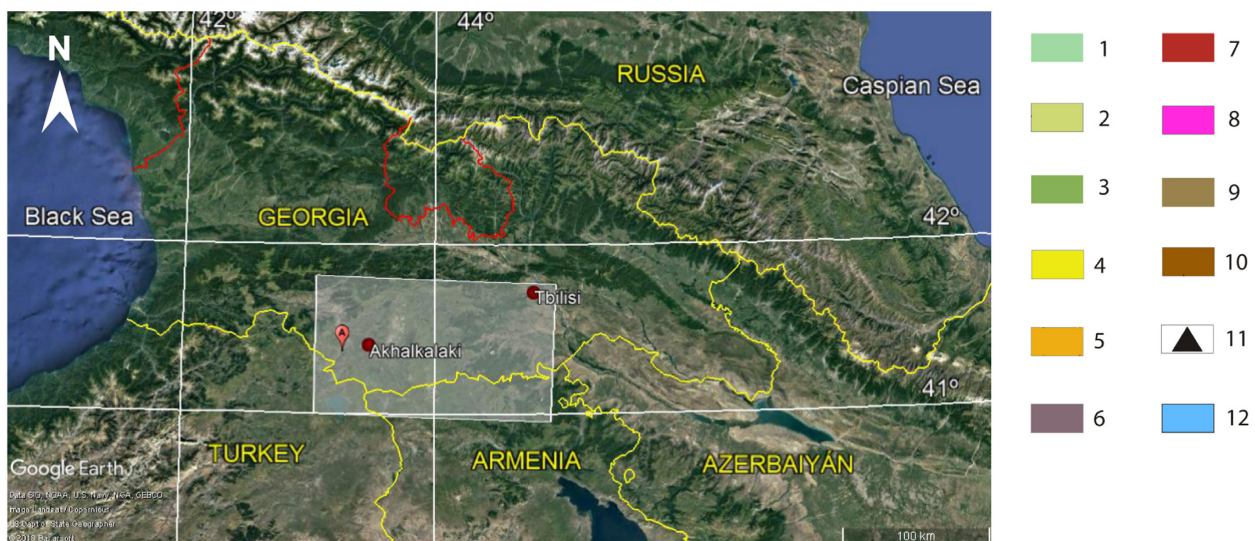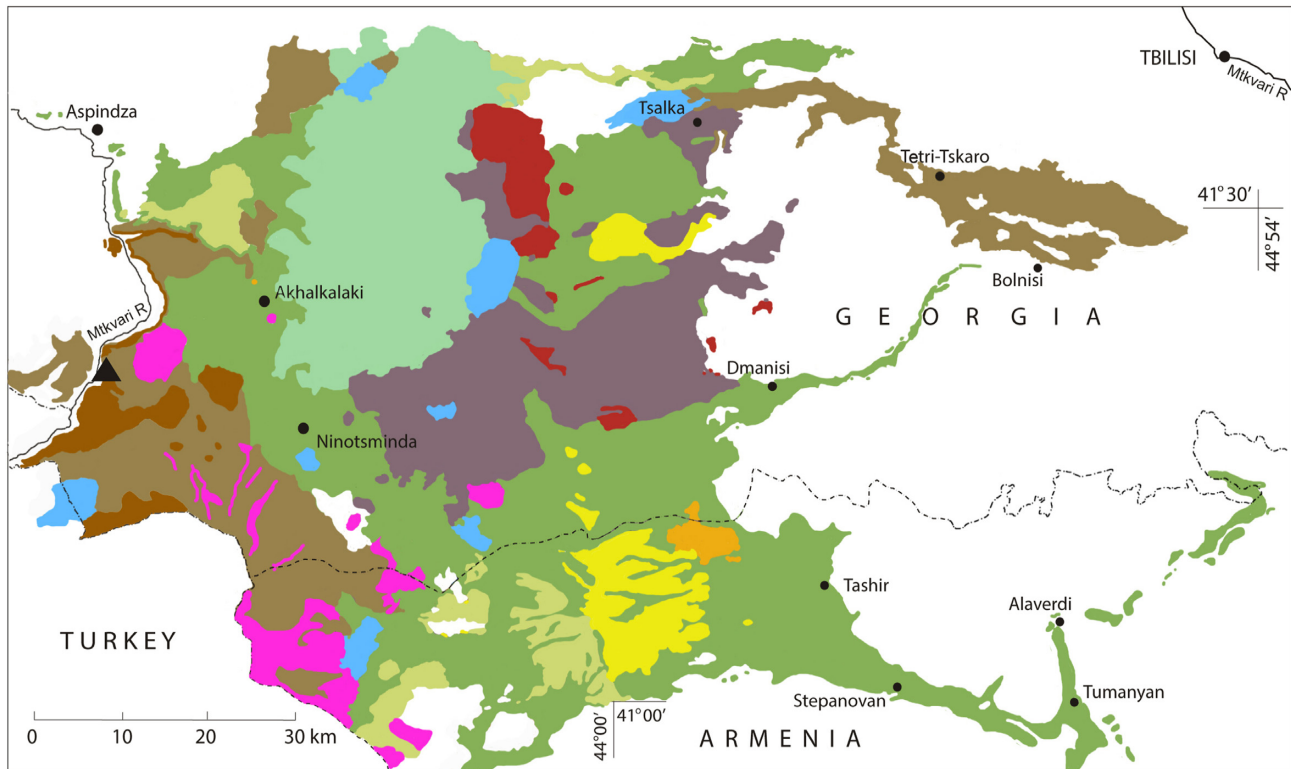
Figure 1. Schematic geological map of the Plio-Pleistocene magmatism in the Djavakheti Highland (Lesser Caucasus) showing lava flow sequences sampled in the present study (taken from Sánchez-Moreno *et al.* 2018; and modified from Lebedev *et al.* 2008; Lebedev 2015). 1 – Quaternary volcanic rocks (andesites and dacites) of the Samsari ridge (800–0 ka); 2–10 Pliocene—Early Quaternary volcanic rocks of Akhalkalaki formation: 2 – Basic lavas (1.75–1.40 Ma), 3 – Basic lavas (2.15–1.95 Ma), 4 – Later dacites and rhyolites of the Javakheti ridge (2.25 Ma), 5 – Hyalodacite (2.5 Ma), 6 – Basic lavas (2.65–2.45 Ma), 7 – Earlier rhyolites and dacites of the Djavakheti ridge (2.85–2.6 Ma), 8 – Dacites of the SW part of Djavakheti highland (3.15–3.11 Ma), 9 – Basic lavas (3.22–3.04 Ma), 10 – Basic lavas (3.75–3.55 Ma), 11 – Sampled lava flow sequences of Apnia, 12 – Lakes. Location map from Google Earth: Image Landsat/Copernicus © 2018 Basarsoft, U.S. Dept. of State Geographer.

3.70 ± 0.20 Ma for flow AP11 (Lebedev *et al.* 2008). In a previous palaeomagnetic study the Apnia sequence has been described as a polarity transition record (Sánchez-Moreno *et al.* 2018). The transition recorded would be either Gilbert–Gauss or a composite transition from chron C2Ar to subchron C2An-2n based on its age. However, a record of non-averaged PSV cannot be dismissed, and is not incompatible with the first interpretation.

3 PREVIOUS ROCK MAGNETIC AND PALAEOMAGNETIC RESULTS

Rock magnetic experiments performed in a previous palaeomagnetic study by Sánchez-Moreno *et al.* (2018), including IRM acquisition and backfield curves, hysteresis loops and strong field magnetization versus temperature (M_S–T) curves, point to titanomagnetite

with varying proportions of titanium and so-called 'pseudo-single-domain' (PSD) grain size as the main carrier of the magnetization in the Apnia samples. Samples were grouped by spatial proximity and representative specimens were taken for the rock magnetic experiments to obtain the most representative magnetic characteristics of each flow.

M_S–T curves observed by Sánchez-Moreno *et al.* (2018) allowed us to distinguish the following behaviour types (Fig. S2): Type H magnetic samples are characterized by quasi-reversible curves and a single high Curie temperature (T_C) mineral phase near 580 °C, corresponding to low-Ti titanomagnetite/magnetite. Type H∗ samples show a similar behaviour as type H samples, with the same low-Ti titanomagnetite phase but initial and final magnetization differed by more than ±15 per cent. M_S–T curves with successive heatings to peak temperatures of 300, 400 and 500 °C show that below these temperatures H∗ samples are reversible. In some cases, very weak phases with T_C around 615 °C appear. This phase might be attributed to the presence of oxidized magnetite (maghemitization). Type L samples display irreversible behaviour and two mineral phases. The first phase matches high-Ti titanomagnetite, appearing in the heating curve between 190 and 280 °C. The second phase is a high T_C phase observed in both heating and cooling curves, which is interpreted as low-Ti titanomagnetite and represents a tiny fraction of the initial magnetization. Type M samples also show an irreversible behaviour and two phases can be distinguished, low-Ti titanomagnetite and an intermediate T_C phase within the 320 to 440 °C range, likely high-Ti titanomagnetite. On other hand, the inflection at about 320 °C could be titanomaghemite, generated by the oxidation of the titanomagnetite.

Hysteresis parameters (Fig. S3) depicted in a Day plot (Fig. S4) have M_{rs}/M_s values ranging from 0.5 to 0.1, showing what has been referred to as 'pseudo-single domain' (PSD) behaviour. However, as pointed out by Roberts *et al.* (2018), Day plots do not allow a simple and direct interpretation of domain states because of the number of variables that influence the hysteresis curve values. Furthermore, Santos & Tauxe (2019) showed that hysteresis parameters have little relationship to reliability of palaeointensity results. In this study, type M and L thermomagnetic curves showed a mixed composition including magnetite, but also titanomagnetite or titanomaghemite with higher Ti content. However, IRM acquisition curves pointed to mainly low coercivity ferrimagnetic phases as carriers of remanence (Sánchez-Moreno *et al.* 2018), ruling out mixtures of phases with very different coercivities. According to Dunlop (2002), theoretical model curves for single-domain (SD) and multidomain (MD) mixtures match the data for PSD magnetite or titanomagnetites with higher Ti contents (titanomagnetites of composition $x = 0$, 0.2, 0.4 and 0.6), although the SD/MD transition region in grain size is much narrower for titanomagnetite with higher Ti contents than for magnetite without titanium. Thus, the PSD behaviour of the studied specimens (Fig. S4) might be explained by a mixture of SD and MD particles although this interpretation is non-unique.

The analysis of palaeomagnetic directions and available radiometric data has established that the Apnia sequence records a polarity reversal between 3.75 ± 0.25 and 3.09 ± 0.10 Ma (Sánchez-Moreno *et al.* 2018). Starting from the base of the section, a succession of 14 reverse polarity lava flows has an average pole that does not match the expected one, which owing to the young age of the sequence is essentially that of a geocentric axial dipole (GAD). The synthetic European apparent polar wander curve (APWP) for the 5 Ma window proposed by Besse & Courtillot (2002) predicts a clockwise deviation of ∼17° in declination and a difference of 2° in inclination for the location. The expected pole is shown in Fig. 2 and

is significantly different from the virtual geomagnetic poles (VGPs) calculated for the lava flows from this study. A single lava flow above the 14 reverse polarity ones records a 'transitional' polarity, with an intermediate VGP latitude of 12.5°. Above this flow, there are five normal polarity flows, which are neither antipodal to the reverse sequence, nor coincident with the expected field direction, and show a counter-clockwise rotation of 27.3°. The possibility of two consecutive rotations in opposite directions in a period between 3.75 and 3.1 Ma seems rather unlikely, hence tectonic rotations are rejected. Directional results do not reflect an EMF behaviour as given by a completely stable polarity record and could indicate a polarity transition. According to the radiometric ages, the sequence was interpreted as recording the reverse to normal Gilbert–Gauss reversal or the C2An-2r to C2An-2n one (upper Mammoth transition) within the Gauss chron. A record of a composite transition cannot be rejected, given that a hiatus described by Lebedev *et al.* (2011) may coincide in age with the three reversals. The hiatus is located between the phases I (3.75–3.55 Ma) and II (3.30–3.05) of Pliocene volcanism recognized in Djavakheti region. Hence, the reverse lower section would correspond to Chron C2Ar (Gilbert) and the normal upper one to C2An-2n. On the other hand, the mismatch with the pole and the high dispersion could be caused by palaeosecular variation (PSV) not being averaged in the record. This second interpretation is supported by the number of directional groups calculated to include the lava flows that show statistically identical palaeomagnetic direction: three for the reverse section, one for the transitional lava flow and three for the normal polarity section. Both interpretations, polarity reversal record and non-averaged PSV record are not mutually exclusive (Sanchez-Moreno *et al.* 2018).

4 PALAEOINTENSITY METHODS

In this study, two different Thellier type methods, Thellier–Thellier (TT, Thellier & Thellier 1959) and IZZI (Yu *et al.* 2004) have been carried out for absolute palaeointensity determinations. Thellier type experiments are based on the progressive replacement of the original thermoremanence (TRM) by partial thermal remanences (pTRMs). Consecutive double stepwise heating with and without applied laboratory field (B_{lab}) according to the chosen protocol are performed.

In the TT method (Thellier & Thellier 1959), specimens are heated and cooled twice, in antiparallel laboratory fields, increasing temperatures at each successive pair of steps. The first heating-cooling cycle at a given temperature (T1) is carried out while applying a laboratory field B_{lab} parallel to the z-axis; during the second cycle at T1 the laboratory field B_{lab} is applied in the opposite direction. B_{lab} was set at 40 μT. Lower temperature steps were repeated (the so-called pTRM checks) to assess the occurrence of magnetochemical alterations. An advantage of this method is that both in-field steps are energetically equivalent, which does not happen in other Thellier-type methods in which zero field steps are performed. TT palaeointensity determinations were carried out in the palaeomagnetic laboratory of the University of Burgos. Small cylindrical specimens subsampled (8 mm diameter) from oriented standard samples were used. Heating-cooling in-field routines were carried out under argon atmosphere, specifically aimed at minimizing oxidation of the samples in the TD48-SC (ASC) thermal demagnetizer. Samples were allowed to cool naturally over several hours. The magnetization was measured using a superconducting magnetometer (2 G Enterprises). Note that during measurement,
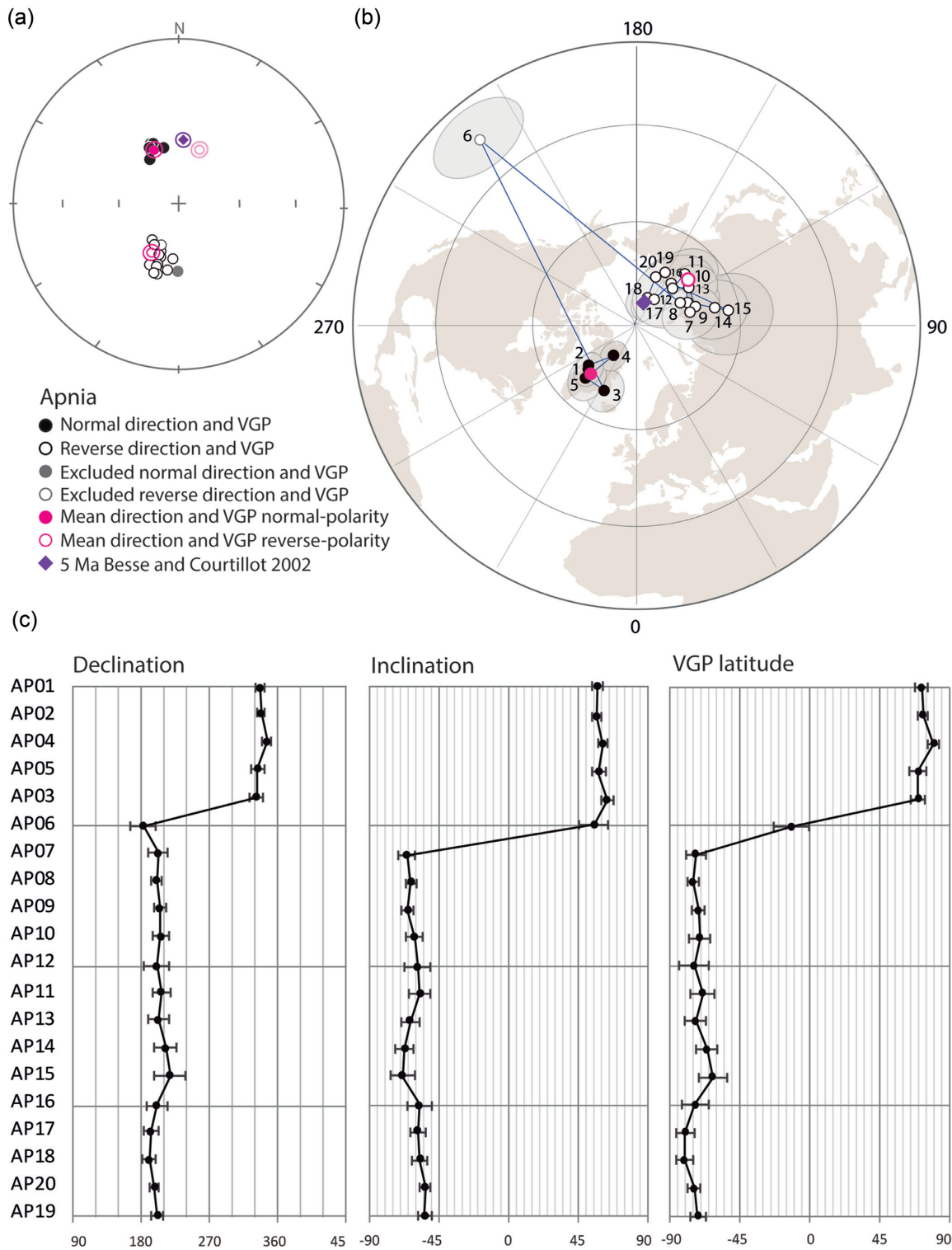
Figure 2. Palaeomagnetic results of the Apnia sequence (Sánchez-Moreno *et al.* 2018). (a) Stereographic projection of mean palaeomagnetic directions (ChRMs) of each lava flow. Normal and reverse directions averages and their α_{95} in pink (reverse average is projected in both north and south hemispheres). Expected direction (Besse & Courtillot 2002) in purple. (b) Stereographic projection of Virtual Geomagnetic Poles. Normal and reverse polarities averages in pink. Expected pole for the last 5 Ma in Eurasia (Besse & Courtillot 2002) in purple. (c) Declination and inclination of palaeomagnetic directions, and VGP latitudes, stratigraphically ordered. Figure taken from Sánchez-Moreno *et al.* (2018).

in several cases difficulties appeared in exactly preserving specimen orientation. Nevertheless, most specimens could be handled correctly, and accurate measurements were obtained.

The IZZI (Yu *et al.* 2004) method provides information about so-called pTRM tails attributed to the presence of grains that fail Thellier's Law of reciprocity (Thellier & Thellier 1959) whereby the unblocking temperature of a component of remanence should be equal to the blocking temperature (a key requirement of palaeointensity determinations). The protocol consists of a sequence of alternating double-heating steps: in field and zero field (IZ), heating and cooling at T1, followed by zero field and in field (ZI) at T2, and so on. The laboratory field, B_{lab}, was also set to 40 μT and pTRM checks (Coe 1967) were also performed. The IZZI method is extremely sensitive to the presence of the pTRM tails, which make the Arai diagrams of specimens whose remanence fails the reciprocity requirement 'zig-zag' (Yu *et al.* 2004; Yu & Tauxe 2005), allowing detection and elimination of unsuitable specimens. Measurements with the IZZI protocol were carried out in the palaeomagnetic laboratory at Scripps Institution of Oceanography, UCSD (USA). In this case, small irregular fragments were taken from standard samples and were prepared in 10 mm diameter vials, previously marked to keep the orientation. The in-house built single chamber thermal demagnetizer and a superconducting magnetometer (2 G Enterprise) were used for these measurements.

Pre-selection criteria applied to the chosen samples, for the Thellier-type methods, were the following (i) $M_S–T$ curves should be reasonably reversible (types H and H∗), (ii) a single primary palaeomagnetic component could be isolated and (iii) at least about 40 per cent of the magnetization still retained at 400 °C in demagnetization experiments for the TT and 60 per cent for the IZZI protocol. Note that the protocols of the two experiments are slightly different in this last point, although not substantially. The criteria are broad, since they are pre-selection, they adapt to the type of samples studied and try to exclude less appropriate cases. As previously mentioned, rock magnetic experiments (Sánchez-Moreno *et al.* 2018) suggest the presence of titanomagnetites which plot in the region of the Day plot previously interpreted as 'PSD' (Fig. S4). One of the possible interpretations of this behaviour is a mixture of SD and MD grains (Dunlop 2002), with a significant amount of the samples plotting near MD values, although the mixing curve did not go through any of our data (supplemental information for Sanchez-Moreno *et al.* 2018). This is interesting as one of the two Thellier-type methods chosen (IZZI) is especially sensitive to the failure of reciprocity, which often is observed in grain populations larger than SD. It should be borne in mind that several other domain state configurations also plot in the PSD area (Roberts *et al.* 2018) and use of Day plots for domain state interpretation is fraught with difficulty. Moreover, Santos & Tauxe (2019) have shown that while the loose designation of 'PSD' has little predictive value for success in palaeointensity experiments, samples with higher ratios of saturation remanence to saturation tend to perform better and those with lower ratios tend to perform worse, there is considerable overlap in behaviours.

Results were considered reliable depending on a set of selection criteria to assess the quality of the experiment conditions, the absence of alteration and the amount of magnetization carried by SD grains. The proposed quality criteria set has been taken from Cromwell *et al.* (2015a), and two arrays of limit values have been selected to distinguish between two quality levels: The stricter thresholds applied to the selected criteria, are also based on Cromwell *et al.* (2015a) and are referred to here as CCRIT (Tauxe *et al.* 2016),

while the more relaxed ones, are called here RCRIT. Threshold values of the 'relaxed' version are however still stricter than those from other frequently used sets of criteria (e.g. Kissel & Laj 2004; Leonhardt *et al.* 2004). The CCRIT and RCRIT criteria and thresholds are the following (to more extensive definitions see Paterson *et al.* (2014)—Standard Palaeointensity Definition):

(1) $n_{measure} \geq 4$, the number of points on an Arai diagram used to estimate the best-fitting linear segment and the palaeointensity.

(2) FRAC ≥ 0.78 and 0.6, NRM fraction used for the best fit on an Arai diagram determined entirely by vector difference sum calculation (Shaar & Tauxe 2013).

(3) $\beta \leq 0.1$, a measure of the relative data scatter around the best-fitting line and is the ratio of the standard error of the slope to the absolute value of the slope (Coe *et al.* 1978).

(4) SCAT = True, Boolean operator which uses the error on the best-fitting Arai plot slope to indicate whether the data over the selected range are too scattered (Shaar & Tauxe 2013). This statistic provides a test for the scatter of the points on the Arai plot, pTRM checks and pTRM tail checks.

(5) gmax ≤ 0.6, the maximum gap factor (g) between two points determined by vector arithmetic (Shaar & Tauxe 2013). g is a measure of the average NRM lost between successive temperature steps of the segment chosen for the best-fitting line on the Arai plot and it reflects the average spacing of the selected points.

(6) k′ ≤ 0.164 and 0.3, the curvature of the Arai plot is determined by the best-fitting circle to all of the data (Paterson 2011), normalized by the respective maximums of the segment NRM and TRM.

(7) $MAD_{Free} \leq 5°$ and 12º, maximum angular deviation (MAD) of the free-floating, directional fits to the palaeomagnetic vector on a vector component diagram (Kirschvink 1980).

(8) DANG $\leq 10°$, (*Deviation ANGle*) the angle between the free-floating best-fitting direction and the direction between data centre of mass and the origin of the vector component diagram (Tanaka & Kobayashi 2003; Tauxe & Staudigel 2004).

(9) $n_{pTRM-check} \geq 2$, the number of pTRM checks used to analyse the best-fitting segment on the Arai plot.

At the site level, the CCRIT threshold values require that the number of specimens $n_{SITE,} \geq 3$ and the standard deviation at the site level $\sigma_{site} \leq 4$ μT and 6 μT or $\sigma_{site} \leq 10$ and 15 per cent of the mean. The Thellier_GUI (Shaar & Tauxe 2013) in the PmagPy package software (Tauxe *et al.* 2016) was used for the interpretation of results obtained with both protocols.

To assess the robustness of our respective criteria CCRIT and RCRIT we evaluate all interpretations for specimens from the Apnia sequence that met these criteria. Then, a bootstrap-like procedure was used, whereby three of the interpretations per site were selected at random and their mean was calculated. If the resulting 'site mean' passed the site level criteria for standard deviation, these were included in the 'accepted site means'. This procedure was repeated 1000 times. The simulated results were compared with the expected field at each site. They are plotted in Fig. 3(a) as red circles or white squares for the RCRIT and CCRIT criteria, respectively. The R^2 value (coefficient of determination of the linear regression) of the RCRIT was 0.92, while that for CCRIT was 0.94. It is likely that for the strongest field, the results suffer a non-linear TRM acquisition and the ancient field was underestimated.

The differences between the calculated and expected fields for the 1000 simulated site means are plotted in Fig. 3(b). The median difference for RCRIT was -2 μT, while that for CCRIT was less than 1 μT and the range of differences for RCRIT was -14.8 to $+15.5$ μT
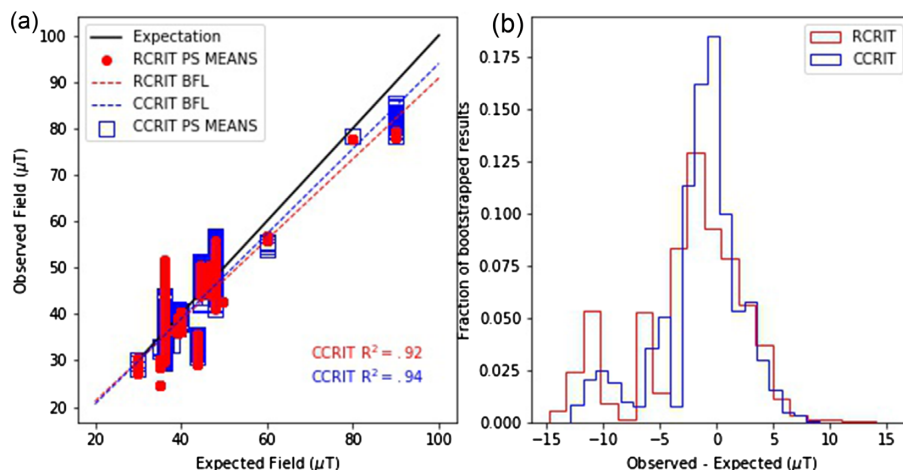
Figure 3. (a) Comparison of estimated intensity values using the sets of selection criteria CCRIT and its relaxed version RCRIT for 1000 bootstrapped samples of Apnia data set. The R^2 values of the linear regressions are shown. CCRIT and RCRIT both perform reasonably well, with CCRIT slightly better than the more relaxed set of criteria. (b) Differences between the calculated and expected fields for the 1000 simulated site means plot.

while that for CCRIT was -12.9 to $9.0\ \mu$T. It is therefore evident that while the stricter criteria do outperform the more relaxed version, the penalty is not very large.

5 RESULTS

In order to obtain a full image of the palaeointensity record, the measurements with the different methods have been carried out trying to include the maximum number of lava flows of the sequence. However, the number of analysed samples was, limited by pre-selection criteria, i.e. mineralogical characteristics and thermal behaviour of the analysed samples.

A total of 55 mini-samples were subjected to the original palaeointensity determination protocol proposed by Thellier & Thellier (1959). The samples were taken from all lava flows of the sequence. In most cases three determinations per flow were performed, except for those in which thermomagnetic curves of some specimens yielded two mineral phases (M and L type), in which case fewer could be carried out. None of the TT experiments passed the strict CCRIT thresholds (Table 1). The somewhat relaxed RCRIT threshold values allowing slightly more scattered directions and somewhat more curved results with a slightly lower fraction of remanence yielded four acceptable TT interpretations from lava flows AP04, AP14 and AP18 (Table 1). Problems in keeping some specimen orientations during TT experiments occurred (see Fig. 4d). This resulted in MAD and DANG values in excess of even the relaxed thresholds RCRIT for acceptance. These results, together with the curved Arai plots, finally have only allowed four TT determinations that could be taken for the flow-averages. Examples of representative experiments are shown in Figs 4(a)–(d). Interestingly, the primary reason for failure of the TT experiments for lava flows with successful IZZI experiments (see below) was curvature (the k' criterion of Paterson *et al.* 2014), due to poorer laboratory handling. Santos & Tauxe (2019) showed that curvature greater than 0.164 was associated with lower precision of palaeointensity estimates, which if too few specimens were analysed could lead to less accurate results.

A total of 100 specimens from all 20 flows that constitute the Apnia sequence were chosen for palaeointensity experiments with the IZZI method (Yu *et al.* 2004). A minimum of two determinations per flow were performed, in some cases even from the same

core, and depending on the sample availability, up to eight. Results of representative experiments are shown in Fig. 4. A total of six specimens from three lava flows (AP04, AP14 and AP18) passed the CCRIT thresholds. As the CCRIT criteria also require at least three specimens from each lava flow to pass and to agree with one another within some tolerance, none of the experiments conducted here pass the strict CCRIT criteria. Using the looser RCRIT criteria, 41 specimens from ten lava flows (AP01, AP04, AP07, AP11, AP14, AP16, AP17, AP18, AP19 and AP20, Table 1) yield acceptable palaeointensity determinations (Fig. 5).

There is no significant theoretical difference between the classical TT and the IZZI methods. Under ideal conditions, both should yield identical answers and if the data are treated in a consistent manner, they can be combined at the site level and analysed jointly. Therefore, we combined the two data sets and ran the Thellier GUI auto interpreter (Shaar & Tauxe 2013) optimizing the standard deviation at the site level to choose from the acceptable interpretations. The only exception was flow AP16, in which, as will be explained below, results were interpreted manually. With this procedure, a total of eight sites passed RCRIT criteria, with a maximum standard deviation at the site level of 4.3 μT and three to eight acceptable specimens per flow (see Table 2).

6 DISCUSSION

6.1 Data analysis

The analysis of palaeointensity data can be very sensitive to interpretation, and for this reason, a strict set of quality criteria has been applied automatically. However, there are cases in which it is necessary to perform an analysis 'by hand' of the possible results, as long as it is based on rigorous and objective criteria. In the analysis of Apnia sequence data we have found some examples in which it is necessary to examine the results by lava flow visually. This was the case of flow AP16. As mentioned in Section 5, the average for the AP16 flow has been calculated manually. This flow yields seven determinations that meet the relaxed selection criteria, but two of them show suspicious two-slope Arai plots and the palaeointensity obtained is significantly greater than in other flows of the sequence. Therefore, these two determinations have been rejected by the automated analysis. For the remaining determinations of the flow, the

Table 1. Successful palaeointensity determinations obtained with the TT and IZZI methods. *site:* Lava flow name. *spec.*: Specimen sub-name. *meth.*: palaeointensity determination method. *Tmin, Tmax*: Minimum and maximum temperature used for the determination. B_{anc}: Palaeointensity value. *n:* Number of experiment steps used in the determination. Experimental statistics: *FRAC, β, gmax, |k′|, MAD, DANG, $n_{pTRMchecks}$* (see the Standard Palaeointensity Definitions (Paterson *et al.* 2014)).

Site	Spec.	Meth.	Tmin (°C)	Tmax (°C)	B_{anc} (uT)	σB_{anc} (μT)	n	β	frac	gmax	|k′|	MAD	DANG	$n_{pTRM\text{-checks}}$
AP01	06B3	IZZI	450	600	38.3	0.8	9	0.02	0.62	0.3	0.027	3.0	1.3	5
AP04	01B3	IZZI	450	580	33.3	2.3	5	0.07	0.61	0.4	0.268	2.6	1.2	4
AP04	01C3	IZZI	450	600	31.9	0.3	9	0.01	0.69	0.3	0.000	3.2	1.8	5
AP04	02B3	IZZI	500	600	34.3	0.7	7	0.02	0.60	0.3	0.026	5.3	1.5	5
AP04	02B4	IZZI	500	600	34.5	1.0	5	0.03	0.63	0.3	0.106	4.6	2.3	4
AP04	03B3	TT	0	582	26.6	1.3	10	0.05	0.97	0.2	0.296	11.5	8.3	4
AP07	03B3	IZZI	400	600	18.0	0.7	10	0.04	0.65	0.3	0.139	5.8	4.8	5
AP07	06B4	IZZI	450	580	18.7	0.7	5	0.04	0.64	0.4	0.191	5.7	4.9	4
AP11	01B3	IZZI	400	600	29.3	0.9	10	0.03	0.62	0.3	0.277	8.3	3.6	5
AP11	01B5	IZZI	450	600	28.9	1.7	6	0.06	0.63	0.4	0.286	3.9	3.2	4
AP11	03A4	IZZI	350	600	22.2	0.9	8	0.04	0.72	0.3	0.299	5.3	5.1	4
AP14	01A3	IZZI	300	600	19.1	0.4	12	0.02	0.75	0.2	0.064	6.6	2.7	5
AP14	03A3	IZZI	300	570	19.8	0.4	10	0.02	0.71	0.2	0.163	4.2	3.9	4
AP14	04B3	IZZI	200	525	19.8	0.2	8	0.01	0.61	0.2	0.045	8.3	7.6	3
AP14	05B3	TT	142	582	20.5	0.6	11	0.03	0.84	0.2	0.050	8.9	9.0	5
AP14	06B3	TT	351	582	20.1	1.0	9	0.05	0.61	0.2	0.250	11.6	6.7	5
AP14	07B3	IZZI	200	525	19.9	0.2	8	0.01	0.64	0.2	0.064	8.7	3.9	3
AP14	08B3	IZZI	0	600	19.8	0.4	14	0.02	0.96	0.2	0.014	5.3	1.7	5
AP14	08B4	IZZI	350	600	19.4	0.8	8	0.04	0.65	0.3	0.065	2.1	2.1	4
AP16	03B3	IZZI	0	500	54.7	3.8	8	0.07	0.66	0.3	0.127	11.4	9.4	2
AP16	05B3	IZZI	0	500	51.8	3.1	8	0.06	0.68	0.3	0.167	11.6	9.2	2
AP16	07A3	IZZI	350	600	17.9	0.4	11	0.02	0.61	0.2	0.159	8.7	5.8	5
AP16	07A4	IZZI	350	600	18.7	0.6	8	0.03	0.67	0.3	0.129	4.2	4.4	4
AP16	07A5	IZZI	350	600	18.9	0.2	8	0.01	0.72	0.2	0.047	5.2	3.3	4
AP16	07B3	IZZI	350	600	14.8	0.9	8	0.06	0.63	0.3	0.270	3.5	2.8	4
AP16	07B4	IZZI	350	600	13.7	0.7	8	0.05	0.63	0.2	0.232	7.7	6.2	4
AP17	01B3	IZZI	400	600	25.7	0.5	10	0.02	0.61	0.2	0.217	7.9	3.9	5
AP17	01B4	IZZI	400	600	27.9	1.1	7	0.04	0.65	0.3	0.284	7.1	4.0	4
AP17	01B5	IZZI	400	600	25.9	1.0	7	0.04	0.62	0.3	0.239	6.1	2.3	4
AP17	04B3	IZZI	300	600	20.3	0.6	12	0.03	0.78	0.2	0.247	9.6	5.8	5
AP17	04B4	IZZI	400	600	18.7	0.9	7	0.05	0.67	0.3	0.296	8.7	7.1	4
AP17	08B3	IZZI	350	580	17.8	0.7	10	0.04	0.62	0.2	0.297	7.0	8.7	5
AP18	02B3	TT	351	582	24.7	0.5	9	0.02	0.63	0.3	0.039	9.8	9.6	5
AP18	03B3	IZZI	300	600	24.3	0.5	12	0.02	0.63	0.2	0.138	8.7	5.1	5
AP18	05B3	IZZI	300	580	23.6	0.9	11	0.04	0.75	0.2	0.299	8.8	7.7	5
AP18	05B4	IZZI	350	560	23.7	1.2	6	0.05	0.64	0.3	0.293	5.4	5.8	3
AP18	05B5	IZZI	350	560	24.0	1.4	6	0.06	0.61	0.3	0.238	3.1	2.5	3
AP19	02B3	IZZI	350	600	20.1	0.6	11	0.03	0.87	0.2	0.172	5.5	3.5	5
AP19	03B3	IZZI	475	580	21.1	0.6	7	0.03	0.62	0.3	0.000	3.6	3.1	5
AP19	05B3	IZZI	500	600	21.2	0.0	7	0.00	0.61	0.4	0.009	4.3	2.9	5
AP19	07A3	IZZI	450	580	21.9	0.7	8	0.03	0.62	0.3	0.144	5.5	2.3	5
AP19	07A4	IZZI	500	600	20.7	0.8	5	0.04	0.61	0.4	0.177	6.7	4.9	4
AP20	01B3	IZZI	350	570	19.4	0.8	9	0.04	0.63	0.2	0.266	7.7	6.0	4
AP20	04A3	IZZI	200	550	19.4	0.8	9	0.04	0.72	0.2	0.274	7.6	9.6	3
AP20	06A3	IZZI	300	560	19.4	0.8	9	0.04	0.65	0.2	0.220	6.2	6.3	4

interval of 350–600 °C has been taken to optimize the adjustment to the requirements per site. Another special case is the flow AP17. The mean palaeointensity obtained shows a standard deviation of 4.3 μT, which corresponds to 18.9 per cent. This high percentage is due to two differentiated groups of three specimens each, the first one around 27 μT and the second one around 18 μT. We have decided to take the average of all six determinations because they are all of high quality and the result obtained is consistent with the results in whole sequence. Note also that AP04 displays one lower palaeointensity value of 26.6 μT, which technically is included, but without it, the flow average would be increased. Two flows, AP01 and AP07 yield valid data, but do not meet the minimum of three determinations per site, so that they had to be excluded.

Finally, eight mean flow palaeointensity values have been obtained from this work. In this study, application of the usual criteria (e.g. Kissel & Laj 2004; Leonhardt *et al.* 2004), would yield a greater number of apparently reliable results. However, this work is focused on obtaining data of high reliability and quality. Given their trustworthiness and robustness, the palaeointensities obtained under the proposed especially strict quality criteria should be especially useful for the development of EMF models.

There are additional factors that could cause significant bias to site averaged palaeointensity results (sites are different lava flows, in our case). Biggin & Paterson (2014b) and Kulakov *et al.* (2019) propose a new set of qualitative criteria (Q_{PI}) to assess the data reliability. They identify several biasing agents applicable to palaeointensity measurements which sometimes are not taken in account in
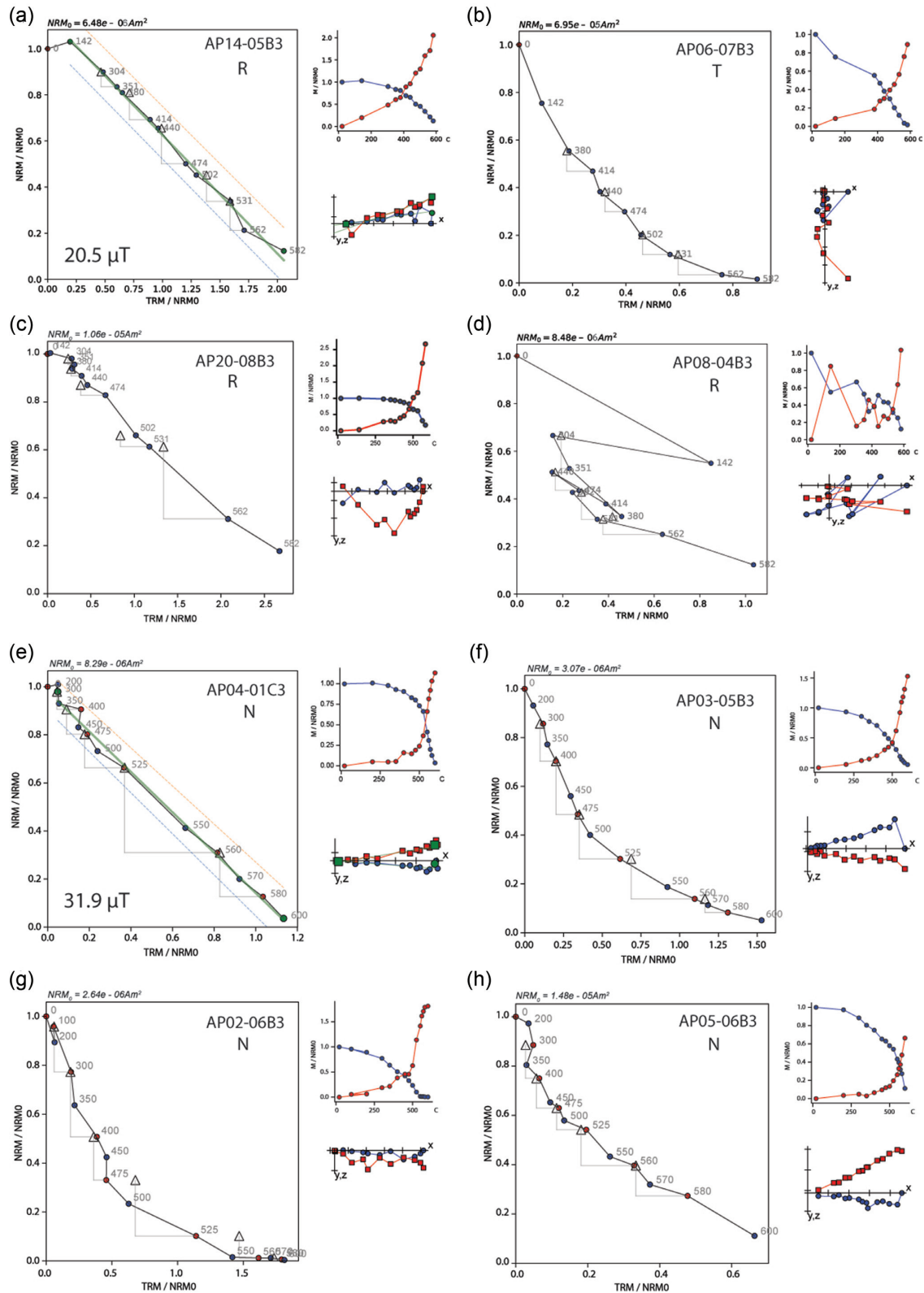
Figure 4. Representative Thellier–Thellier and IZZI experiments. Different behaviours are shown for TT (a–d) and IZZI (f–i): Successful determinations (a and e), passed the RCRIT acceptance criteria and the best-fitting line is shown in solid green. The SCAT criterion is plotted as dotted lines. Failing determination by the curvature (b and f), determination with magnetochemical alteration (c and f), no orientation kept during measurements (d) and zig-zag behaviour of the MD (h). Upper figures are the Arai plots (Nagata *et al.* 1963). Lower-right ones are the Zijderveld plots (Zijderveld 1967). The blue circles are horizontal projections of the zero field steps after adjusting the NRM value of x to be zero, red squares are the X and Z vertical projections. Lower-left figures are the magnetizations remaining (blue) and gained (red) at each temperature step. N: Palaeointensity from normal polarity lava flow. R: reverse polarity. T: Transitional polarity.
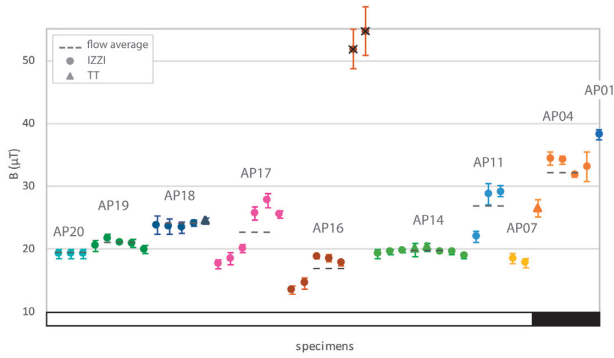
Figure 5. Plot of specimen data by lava flow. Triangles (circles) are the IZZI (Thellier–Thellier) results. Individual results crossed out have been dismissed. Flow means are plotted as dotted lines.

studies. In the following lines we discuss to which extent our results from the Apnia sequence match with the Q_{PI} criteria.

(1) AGE: Assesses whether the associated absolute age estimate, remanence component structure, and palaeomagnetic direction are consistent with a reliable and useful palaeointensity. Apnia palaeointensity results are linked to reliable K-Ar age and palaeomagnetic behaviour derived from a primary component of remanence (Sánchez-Moreno *et al.* 2018).

(2) STAT: Sufficient number of specimens to test whether the palaeointensity result consistency is reasonable to have a moderate precision ($n_{specimen} \geq 5$). Six lava flows passed the requirement of at least five individual specimens used for the palaeointensity average (AP04, 14, 16, 17, 18 and 19). Two flows have a 3-specimens average (AP11 and 20), which commonly, is still considered a good average.

(3) TRM: The remanence must be thermal so that the palaeointensity acquisition performed in the laboratory is proportional to that produced by the EMF at the time of rock magnetization. Rock magnetic results point to remanence being a TRM in samples used for palaeointensity determinations. The fact that these are lava flows involves a TRM because the volcanic rocks undergo a cooling at the moment of their formation, although we do not have independent petrological evidence.

(4) ALT: Heating induced alteration is a major threat to the accuracy of palaeointensity measurements. pTRM checks and rock-magnetism experiments (thermomagnetic curves) support that there is not alteration in Apnia specimens.

(5) MD: Reasonable evidence that the final estimate was not significantly biased by multidomain behaviour during the experiment. High FRAC parameter (≤ 0.6) verify that the MD effect does not affect the final palaeointensity estimate.

(6) ACN:

(i) Cooling rate: The characteristics of the studied lava flows (thickness, composition, etc., see Section 2) allow the assumption that the cooling-rate does not affect the palaeointensity experiments, given that it does not vary significantly in the range of thickness of the individual cooling units, although (Santos & Tauxe 2019) have shown that cooling rate dependence is difficult to predict. As far as the cooling-rate dependence is concerned, the TT and IZZI experiments have been performed by leaving the samples cool down naturally ($\sim$10 h) and with a fan ($\sim$1 hr), respectively, without differences in the results.

(ii) Anisotropy of TRM: In order to analyse the influence of the anisotropy of remanence on our results, we have used the anisotropy

of magnetic susceptibility (AMS) as a proxy. We measured AMS on one sample from each flow, at the beginning of the palaeomagnetic study of the Apnia sequence, and in all cases a very low anisotropy was observed, with a corrected anisotropy P' value (Jelinek 1981) of approximately 4 per cent (P' between 1 and 1.040, average 1.014). In addition, we calculated the gamma statistic γ (Paterson *et al.* 2014; Standard Palaeointensity Definitions, SPD), which detects in many cases the influence of anisotropic TRM (in the case where the lab field is applied along one of the eigenvectors. The requirement of multiple unoriented specimens guards against this unlikely scenario). Both the TT and IZZI determinations, yielded values between 0.2° and 3.7°. These results suggest that anisotropy of remanence does not play an important role in our samples, as only when gamma $>>4°$ it is considered that there is a higher chance that the specimen is anisotropic (Paterson *et al.* 2015).

(iii) Non-linear TRM effects: The non-linear dependence of TRM on applied field is minimal when the laboratory and ancient field strengths are approximately equal (Selkin *et al.* 2007; Paterson 2013). For most typical geological materials (i.e. lavas) if both fields are within $\sim$1.5 times each other, then the influence of non-linear TRM is likely to be minimal (Biggin & Paterson 2014a).

(7) TECH: Estimate is an average of results from more than one palaeointensity technique. In Apnia sequence, final palaeointensity on three lava flows has been calculated from more than one Thellier-type technique (AP04, 14 and 18), nevertheless TT and IZZI methods are non-independent, so these palaeointensity averages do not meet the criterion.

(8) LITH: Estimate is an average of results from more than one lithology or from samples from the same lithology showing significantly different unblocking behaviour. The palaeointensity estimations in Apnia have been performed over samples of similar lithology and with similar unblocking behaviour.

As a result, six lava flows (AP04, AP14, AP16, AP17, AP18 and AP19) yield $Q_{PI} = 5$ and in only two cases (AP11 and AP20) $Q_{PI} = 4$. According to Biggin and Paterson (2014), 60 per cent of the palaeointensity values collected in the PINT database (updates between 2012.08 and 2014.01) (Biggin *et al.* 2010) show a Q_{PI} score of 1, 2 and 3. The data obtained in the Apnia sequence show a higher quality than the mean, according to the Q_{PI} evaluation methodology.

6.2 Directional results versus palaeointensities

Palaeomagnetic directions of the Apnia sequence might show a (perhaps partial) polarity reversal, or a composite reversal (Sánchez-Moreno *et al.* 2018). According to radiometric ages (Lebedev *et al.* 2008), the sequence could record the reverse to normal C2Ar to C2An-3n (Gilbert–Gauss) polarity change or its reverse lower part could correspond to chron C2Ar and the upper part to C2An-2n. The Apnia sequence is composed of two subsections recording different polarities, which are not antipodal, separated by a single flow with a transitional direction (Fig. 2). Based on the analysis of palaeomagnetic directions, virtual geomagnetic poles scatter, directional groups and a few previously available palaeointensity results (Calvo-Rathert *et al.* 2013), two differing though not conflicting interpretations were proposed for the sequence (Sánchez-Moreno *et al.* 2018): (1) an anomalous EMF record and (2) a short recording time unable to average palaeosecular variation.

Table 2. Averaged palaeointensity by lava flow results. *site:* Lava flow name. *polarity:* VGP polarity obtained to each lava flow. *min age:* K-Ar date obtained from the flows AP01 and AP12. B_{anc}: Palaeointensity value. σ_{site}: Standard deviation by site. *VADM:* Virtual axis dipole moment.

Site	Polarity	Min age (Ma)	B (μT)	n_{SITE}	σ_{SITE} (μT)	σ_{SITE} (%)	VADM (ZAm^2)	σ VADM (ZAm^2)
AP04	N	3.09	32.1	5	3.3	10.1	54.6	5.5
AP11	R	3.70	26.8	3	4.0	14.8	45.6	6.7
AP14	R	3.70	19.8	8	0.4	2.2	33.7	0.7
AP16	R	3.70	16.8	5	2.4	14.3	28.6	4.1
AP17	R	3.70	22.7	6	4.3	18.9	38.7	7.3
AP18	R	3.70	24.1	5	0.4	1.8	40.9	0.7
AP19	R	3.70	21.0	5	0.7	3.2	35.7	1.1
AP20	R	3.70	19.4	3	0.0	0.1	33.0	0.0

6.1.1 Anomalous EMF record (reflecting a polarity reversal or composite reversal)

In this study, palaeointensity values between 16.8 and 26.8 μT in the lower reverse polarity section have been obtained, while a single determination in the upper normal-polarity section yields a higher single value of 32.1 μT. At present, the EMF intensity in Georgia is 49 μT under a presumably stable magnetic field regime, significantly higher than the values obtained for the Apnia lavas. This disagreement could be due to the Apnia lavas being emplaced during a polarity transition as there is a general accord among the palaeomagnetic community that during large deviations of the geomagnetic field from the axial dipole position the intensity decreases (e.g. Valet *et al.* 2005). Another observed characteristic of polarity transitions is that their onset is often first found in the intensity record and later in the directional one (e.g. Prévot *et al.* 1985; Herrero-Bervera & Valet 1999), similarly to the observed low field values in the Apnia lavas before the transitional direction. Considering these references, it is possible to interpret that the lower part of the Apnia sequence records the intensity drop, starting to the reversal, whereas the upper section shows the recovery of the EMF intensity, after the reversal.

Nevertheless, an isolated record of a stable EMF would also be a possible interpretation of the lower section of Apnia sequence if we consider it as independent from transitional and subsequent normal polarity upper section. Besides the lower section show VGPs closer to the expected pole than the upper one (Fig. S2). In fact, the angular dispersion analysis over lower Apnia VGPs with respect to the expected pole, shows values within the range proposed by the PSV models in lavas (Sánchez-Moreno *et al.* 2018).

6.1.2 Short recording time unable to average palaeosecular variation (PSV)

On the other hand, assuming that a limited number of directional groups was determined over the 20 flows of Apnia sequence (three of reverse polarity, one transitional and three of normal polarity), a short time of emplacement for the different flow groups is suggested. It is therefore possible that this low amount of independent data represents snapshots of the field and does not average out secular variation.

We have to be mindful that the term PSV describes temporal variations in the field, meaning not only variations of declination and inclination, but also in intensity. As in directional studies, a non-averaged PSV also indicates that the virtual axial dipole moment (VADM), obtained from the intensity at a specific location, represents a spot image of the EMF variation and cannot be taken as a GAD value for that time. Likewise, the virtual geomagnetic pole

(VGP), corresponding to the EMF direction obtained for the same data, would not represent the GAD. This can lead to confusion with a transitional record, where the GAD is very weak and therefore the VGP does not coincide with the geographic north and the VADM value is anomalous.

Now, the question to be posed is how long the averaged period should be to make sure that a representative value of the time-averaged field is obtained. Traditional analysis of long-term PSV covers periods longer than 10^5–10^6 yr (e.g. Johnson & Constable 1996; McElhinny *et al.* 1996; Merrill *et al.* 1996; Harrison 2007; Johnson *et al.* 2008). However, there are also studies on datasets that cover a smaller timescale. Barton (1982) used sediment records to suggest that timescales of at least 10^3 yr provided reasonable estimates of PSV, as well as studies that suggest at least 10^4–10^5 yr (Carlut *et al.* 1999; Merrill & McFadden 2003), while Lund (2018) considers a scale of 10^3–10^5. Constable & Johnson (2005) perform a power spectrum analyses from 10^7 to 10^2 yr where the spectrum between 10^1 to 10^4 yr is taken to characterize the PSV. Our sequence is in the range of 10^5 yr, which is likely to support a record where the PSV is averaged.

On the other hand, the palaeointensity values obtained in Apnia might also reflect a weak time-averaged field (TAF) during a stable regime. The observed low field strength is not inconsistent with other palaeointensity records for this time period (e.g. Juarez & Tauxe 2000, Wang *et al.* 2015; Cromwell *et al.* 2015a). These are TAF results obtained with high quality palaeointensity data and analysis of the global database MagIC (Tauxe *et al.* 2016) excluding non-ideal data (Juárez *et al.* 1998; Tauxe *et al.* 2013).

6.3 Global VADMs during the 3–4 Ma

Flow-average palaeointensities obtained range from 16.8 to 32.1 μT. Translating intensity values to virtual axial dipole moments (VADM), yields values between 28.6 and 54.6 ZAm^2. The mean for the whole sequence is 38.9 ZAm^2, which is half of the present VADM ($\sim$80 ZAm^2).

Analysis of palaeointensity results of stable polarity periods during the last 5 Myr have come to different conclusions. There are studies suggesting VADM averages of 55 ZAm^2 (Juárez & Tauxe 2000) and 36 ZAm^2 (Yamamoto & Tsunakawa 2005) and (Cromwell *et al.* 2015a) obtained values of 47 ZAm^2 for the last 5 Myr, a similar value as that suggested by Tauxe *et al.* (2004) for the Brunhes–Matuyama transition (49 ZAm^2). On the other hand, older studies based on less restrictive selection criteria resulted in VADM values close to the present one (McFadden & McElhinny 1982; Goguitchaichvili *et al.* 1999; Heller *et al.* 2002; Smirnov & Tarduno 2003). For older and longer periods VADM averages of 42–48 ZAm^2 for the 0–160 Myr
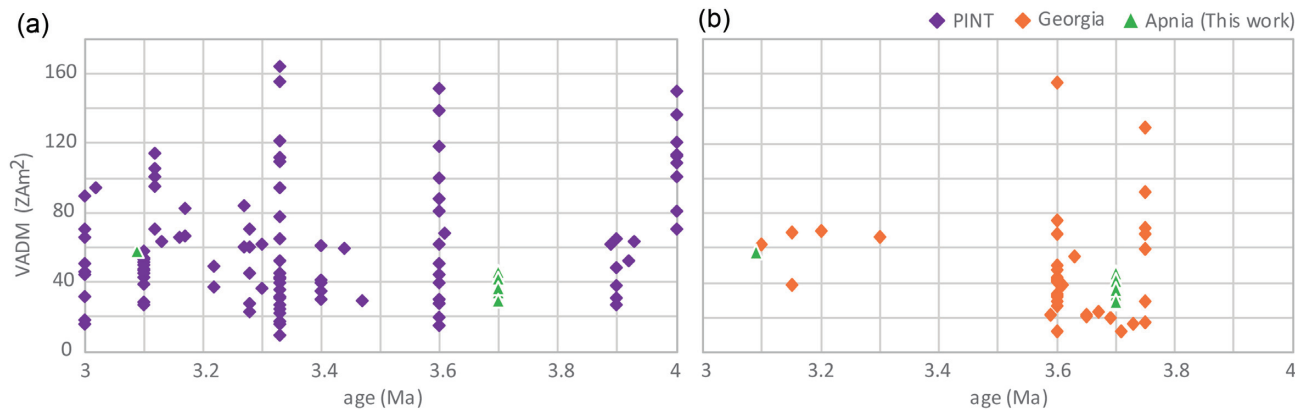
Figure 6. VADM calculated from palaeointensities between 3 and 4 Ma (age range covered by the Apnia sequence), extracted from the PINT2015.05 database (Biggin *et al.* 2010). (a) VADM from different latitudes, excluding Georgia data, plotted together with Apnia results from this study. (b) VADM from the Djvakheti Highland plotted together with Apnia results from this study.

range (Juárez *et al.* 1998; Tauxe 2006; Tauxe *et al.* 2013) have been suggested while the older study of Tanaka *et al.* (1995) estimated the average dipole moment for the last 20 Ma to be approximately 84 ZAm^2. It should be noted that significantly lower values are found in the Mesozoic, during the so-called Mesozoic dipole low (Prévot *et al.* 1990; Perrin & Shcherbakov 1997; Biggin & Thomas 2003), which might reduce the average value in calculations including the last 160 or 300 Myr. Due to the high temporal and spatial variability of the EMF, some caution should be however applied when comparing the results from the short Apnia sequence, which records a period of less than 1 Myr at 40° latitude, with the results from different intervals of the global databases (i.e. PINT; Biggin *et al.* 2010 and MagIC; Tauxe *et al.* 2016). If we separate the values obtained in the normal (upper) and reverse (lower) sequences, considering they are not antipodal and do not match the GAD, we obtain 54.6 and 36.6 ZAm^2 respectively. Therefore, the VADM average of the lower Apnia, prior to the polarity change, is below the most recent estimates of the VADM median value calculated for the last 5 Myr, but comparable to those suggested by Lawrence *et al.* (2009) and Cromwell *et al.* (2015a) from high latitude sites.

The results have also been compared with VADMs obtained in different locations for the 3–4 Ma age interval, which is the period covered by the Apnia sequence (PINT 2015.05, Biggin *et al.* 2010, Table S1 and Fig. 6). The data have been filtered allowing only palaeointensities from Thellier-type methods with pTRM checks. Nonetheless, the selection criteria applied to this data are those commonly used (Leonhardt *et al.* 2004). The results from the Djavakheti Highland have been compared separately and show both higher and equivalent VADM values with respect to this study (Table S1 and Fig. 6b). Calvo-Rathert *et al.* (2011) obtain an average VADM of 66 ZAm^2 on different sequences from the Djavakheti Highland. Calvo-Rathert *et al.* (2013) obtain results on some samples from the Apnia sequence, ranging between 29 and 130 ZAm^2. This last work was performed on specimens sub-sampled from blocks taken in samplings in 1984–1986, in which besides a possible orientation error, no information about the specific stratigraphic order of each lava flow was available. Then, we have used palaeomagnetic information from Calvo-Rathert *et al.* (2013) to try to correlate their results and those of this study (Table S3). Four palaeointensity results have been correlated with the lower section of inverse polarity, thanks to the directional groups obtained in Sanchez-Moreno *et al.* (2018). Values of 76.1 µT (n = 1) and 17.3 µT (n = 5) match the three lowest flows. The second one is clearly in better agreement

with the values obtained in this study and having been obtained from an average of five determinations also can be considered more reliable. Matching with our AP11 flow, Calvo-Rather *et al.* (2013) obtains a similar value of 27.4 µT (n = 2). In the upper normal polarity section we found a coincidence with the directions obtained in flow AP04, but the result obtained by Calvo-Rathert *et al.* (2013) displayed a much higher palaeointensity value (54.3 µT, n = 2). Although in this study we could not obtain results for the transitional polarity flow, Calvo-Rathert *et al.* (2013) obtained a palaeointensity result of 26 µT (n = 1) in Masa flow characterized by a transitional VGP. Thus, only some coincidences can be observed with the study of Calvo-Rathert *et al.* (2013). In other studies performed in the Djavakheti highland, Goguitchaichvili *et al.* (2009) yield the lowest values ranging from 12 to 55 ZAm^2, while Camps *et al.* (1996) obtain, mostly palaeointensities within the range obtained in this work (Table S1 and Fig. 6b). The low intensities observed by Goguitchaichvili *et al.* (2009) and Camps *et al.* (1996) are related to the Gilbert–Gauss reversal, as could be the data from this study.

Regarding locations outside Georgia, 112 VADM data points within the age range of 3–4 Ma have been extracted from the PINT15.05 database (Biggin *et al.* 2010) taking only data from Thellier-type methods with pTRM checks. These data, show a very scattered distribution (Table S1 and Fig. 6a). Therefore, it is not possible to observe any correlation with the data set obtained in this work. This analysis brings to light the problem of the global palaeointensity database which needs to be completed with a more uniform distribution around the globe and uniformity in the quality of the data.

For comparison, we downloaded the palaeointensity measurements available in the MagIC database (Tauxe *et al.* 2016) for the age range 2.5–4.5 Ma (Tauxe & Staudigel 2004; Tauxe *et al.* 2004; Tauxe 2006; Lawrence *et al.* 2009) and reinterpreted them applying the selection criteria set RCRIT, used in this study (Table S2). The number of results, as expected, is far fewer under these stricter criteria than in the original studies (in particular, none of the determinations performed in Calvo-Rathert *et al.* (2013) passes the RCRIT criteria). The VADMs that pass our criteria have an average of 48.6 ZAm^2, higher than those obtained in the lower section of the Apnia sequence (36.6 ZAm^2), prior to the polarity change. This would be in agreement with the intensity drop observed at pre-transitional moments, although an isolated record of a stable EMF cannot be discarded for the lower part of Apnia section. This interpretation would support a weak time-averaged field, although

the effect of non-averaged PSV should also be taken into account. The latter could also apply to the high intensity observed in the upper Apnia section.

7 CONCLUSIONS

An absolute palaeointensity determination study has been carried out on the Pliocene Apnia sequence composed of 20 lava flows. Directional palaeomagnetic results obtained by Sánchez-Moreno *et al.* (2018) on this sequence provide two different though not conflicting interpretations, a short recording time unable to average PSV and/or an anomalous EMF record. The lower reverse polarity Apnia section seems to average the PSV, while the upper normal polarity section shows a wider scatter. According to available radiometric ages, the sequence might record the Gilbert–Gauss transition, although a composite transition record from chron C2Ar to subchron C2An-2n cannot be discarded (Sánchez-Moreno *et al.* 2018).

A total of 55 palaeointensity determinations were carried out using the TT method and 100 with the IZZI method. We obtained four successful TT determinations and 41 IZZI determinations, under the proposed RCRIT thresholds, although none met the stricter CCRIT set. The still very stringent RCRIT set thus allowed a selection of 45 high quality and reliable palaeointensity determinations.

Application of the RCRIT criteria at site level yields average palaeointensity results in eight of the 20 studied lava flows. VADM values between 28.6 and 45.6 ZAm^2 have been obtained in the lower reverse section. The (single) normal polarity determination from the upper section shows, however, a higher value of 54.6 ZAm^2. These values are well below the present-day dipole moment in Georgia (84 ZAm^2) and the mean VADM obtained by Tanaka *et al.* (1995) for the last 20 Myr. On the other hand, more recent studies using stricter criteria have obtained VADM averages for the last 5 Ma between 36 and 55 ZAm^2 (Juarez & Tauxe 2000; Yamamoto & Tsunakawa 2005) in agreement with those obtained in this study in the Apnia sequence.

The relatively low palaeointensity values obtained on the flows erupted before the lava flow that recorded a transitional polarity support the hypothesis that the reverse polarity section of the Apnia sequence recorded a transitional EMF intensity. These results suggest that the palaeointensity drops before the complete directional reversal. The higher value obtained after the reversal depicts the recovery of the EMF intensity, still within an anomalous regime. The data obtained are consistent with the observation that the intensity decreases significantly during polarity reversals (Valet *et al.* 2005) and that this decrease is observed before the onset of directional anomalies (e.g. Prévot *et al.* 1985). The palaeointensity recorded in the normal polarity upper section are slightly higher, probably showing a trend towards a more stable field regime. However, the palaeointensity results obtained in lower Apnia yield data for only seven flows from three directional groups. Thus, an isolated record of a stable EMF cannot be discarded. This interpretation would support a weak time-averaged field, although the effect of non-averaged PSV cannot be excluded.

REFERENCES

Adamia, S., Zakariadze, G., Chkhotua, T., Sadradze, N., Tsereteli, N., Chabukiani, A. & Gventsadze, A., 2011. Geology of the Caucasus: a review, *Turkish J. Earth Sci.,* **20,** 489–544.

Avagyan, A., Sosson, M., Karakhanian, A., Philip, H., Rebai, S., Rolland, Y., Melkonyan, R. & Davtyan, V., 2010. Recent tectonic stress evolution in the Lesser Caucasus and adjacent regions, *Geol. Soc. Lond., Spec. Publ.,* **340,** 393–408.

Barton, C.E., 1982. Spectral analysis of palaeomagnetic time series and the geomagnetic spectrum, *Phil. Trans. R. Soc., A,* **306,** 203–209.

Besse, J. & Courtillot, V., 2002. Apparent and true polar wander and the geometry of the geomagnetic field over the last 200 Myr, *J. geophys. Res.,* **107,** 2300, doi:10.1029/2000JB000050.

Biggin, A.J., McCormack, A. & Roberts, A., 2010. Paleointensity database updated and upgraded, *EOS, Trans. Am. Geophys. Un.,* **91,** 15, doi:10.1029/2010EO020003.

Biggin, A.J. & Paterson, G.A., 2014a. A new set of qualitative reliability criteria to aid inferences on palaeomagnetic dipole moment variations through geological time, *Front. Earth Sci.,* **2,** 1–9.

Biggin, A.J. & Paterson, G.A., 2014b. A new set of qualitative reliability criteria to aid inferences on palaeomagnetic dipole moment variations through geological time, *Front. Earth Sci.,* **2,** 1–9.

Biggin, A.J., Perrin, M. & Dekkers, M.J., 2007. A reliable absolute palaeointensity determination obtained from a non-ideal recorder, *Earth planet. Sci. Lett.,* **257,** 545–563.

Biggin, A.J. & Thomas, D.N., 2003. Analysis of long-term variations in the geomagnetic poloidal field intensity and evaluation of their relationship with global geodynamics, *Geophys. J. Int.,* **152,** 392–415.

Calvo-Rathert, M., Bógalo, M.F., Gogichaishvili, A., Sologashvili, J. & Vashakidze, G., 2013. New paleomagnetic and paleointensity data from Pliocene lava flows from the Lesser Caucasus, *J. Asian Earth Sci.,* **73,** 347–361.

Calvo-Rathert, M., Gogichaishvili, A., Vashakide, G. & Sologashvili, J., 2015. New paleomagnetic and paleointensity data from Georgia (Caucasus): a review, *Latinmag Lett.,* **5,** 1–23.

Calvo-Rathert, M., Goguitchaichvili, A., Bógalo, M.F., Vegas-Tubía, N., Carrancho, Á. & Sologashvili, J., 2011. A paleomagnetic and paleointensity study on Pleistocene and Pliocene basaltic flows from the Djavakheti Highland (Southern Georgia, Caucasus), *Phys. Earth planet. Inter.,* **187,** 212–224.

Camps, P. *et al.*, 1996. Paleomagnetic and geochronological study of a geomagnetic field reversal or excursion recorded in pliocene volcanic rocks from Georgia (Lesser Caucasus), *Phys. Earth planet. Inter.,* **96,** 41–59.

Carlut, J., Courtillot, V. & Hulot, G., 1999. Over how much time should the geomagnetic field be averaged to obtain the mean-palaeomagnetic field ? *Terra Nov.,* **11,** 239–243.

Coe, R.S., 1967. Paleo-intensities of the Earth's magnetic field determined from Tertiary and Quaternary rocks, *J. geophys. Res.,* **72,** 3247–3262.

Coe, R.S., Grommé, S. & Mankinen, E.A., 1978. Geomagnetic paleointensities from radiocarbon-dated lava flows on Hawaii and the question of the Pacific nondipole low, *J. geophys. Res.,* **83,** 1740–1756.

Constable, C. & Johnson, C., 2005. A paleomagnetic power spectrum, *Phys. Earth planet. Inter.,* **153,** 61–73.

Cromwell, G., Tauxe, L. & Halldórsson, S.A., 2015a. New paleointensity results from rapidly cooled Icelandic lavas: implications for Arctic geomagnetic field strength, *J. geophys. Res.,* **120,** doi:10.1002/2014JB011828.

Cromwell, G., Tauxe, L., Staudigel, H. & Ron, H., 2015b. Paleointensity estimates from historic and modern Hawiian lava flows using glassy basalt as a primary source material, *Phys. Earth planet. Inter.,* **241,** 44–56.

Day, R., Fuller, M. & Schmidt, V.A., 1977. Hysteresis properties of titanomagnetites: Grain-size and compositional dependence, *Phys. Earth Planet. Inter.,* **13** (4), 9–22.

Doubrovine, P.V., Veikkolainen, T., Pesonen, L.J., Piispa, E., Ots, S., Smirnov, A.V., Kulakov, E.V. & Biggin, A.J., 2019. Latitude dependence of geomagnetic paleosecular variation and its relation to the frequency of magnetic reversals: observations from the Cretaceous and Jurassic, *Geochem., Geophys. Geosyst.,* **20,** 1240–1279.

Dunlop, D.J., 2002. Theory and application of the Day plot (Mrs/Ms versus Hcr/Hc) 1. Theoretical curves and tests using titanomagnetite data, *J. geophys. Res.,* **107,** EPM4-1–EPM4-22.

Glatzmaier, G.A. & Coe, R.S., 2015. Magnetic polarity reversals in the core, in *Treatise on Geophysics,* pp. 279–295, ed. Schubert, G., Elsevier.

Goguitchaichvili, A., Calvo-Rathert, M., Sologashvili, J., Morales, J., Soler, A.M. & Espinosa, M., 2001. A reconnaissance magnetostratigraphy of Georgian Plio-Quaternary volcanic provinces (southern Caucasus), *Geofis. Int.,* **40,** 111–119.

Goguitchaichvili, A., Cervantes, M.A., Calvo-Rathert, M., Camps, P., Sologashvili, J. & Maissuradze, G., 2009. Gilbert-Gauss geomagnetic reversal recorded in Pliocene volcanic sequences from Georgia (Lesser Caucasus): revisited, *Earth, Planets Space,* **61,** 71–81.

Goguitchaichvili, A. *et al.*, 2000. Palaeomagnetism of Georgian Plio-Quaternary volcanic provinces (Southern Caucasus): a pilot study, *Comptes Rendus l'Académie des Sci. - Ser. IIA - Earth Planet. Sci.,* **331,** 683–690.

Goguitchaichvili, A.T., Prévot, M. & Camps, P., 1999. No evidence for strong fields during the R3-N3 Icelandic geomagnetic reversal, *Earth planet. Sci. Lett.,* **167,** 15–34.

Harrison, C., 2007. Secular variation model, in *Encyclopedia of Geomagnetism and Paleomagnetism,* pp. 892–901, eds Gubbins, D. & Herror-Bervera, E., Springer.

Heller, R., Merrill, R.T. & McFadden, P.L., 2002. The variation of intensity of earth's magnetic field with time, *Phys. Earth planet. Inter.,* **131,** 237–249.

Herrero-Bervera, E. & Valet, J.-P.P., 1999. Paleosecular variation during sequential geomagnetic reversals from Hawaii, *Earth planet. Sci. Lett.,* **171,** 139–148.

Jelinek, V., 1981. Characterization of the magnetic fabric of rocks, *Tectonophysics,* **79,** T63–T67.

Johnson, C.L. & Constable, C.G., 1996. Palaeosecular variation recorded by lava flows over the past five million years, *Phil. Trans. R. Soc. Lond., A,* **354,** 89–141.

Johnson, C.L. *et al.*, 2008. Recent investigations of the 0–5 Ma geomagnetic field recorded by lava flows, *Geochem., Geophys. Geosyst.,* **9,** doi:10.1029/2007GC001696.

Juarez, M.T. & Tauxe, L., 2000. The intensity of the time-averaged geomagnetic field: the last 5 Myr, *Earth planet. Sci. Lett.,* **175,** 169–180.

Juárez, M.T., Tauxe, L., Gee, J.S. & Pick, T., 1998. The intensity of the Earth's magnetic field over the past 160 million years, *Nature,* **394,** 878–881.

Kirschvink, J.L., 1980. The least-squares line and plane and the analysis of palaeomagnetic data, *Geophys. J. R. astr. Soc.,* **62,** 699–718.

Kissel, C. & Laj, C., 2004. Improvements in procedure and paleointensity selection criteria (PICRIT-03) for Thellier and Thellier determinations: application to Hawaiian basaltic long cores, *Phys. Earth planet. Inter.,* **147,** 155–169.

Kulakov, E.V. *et al.*, 2019. Analysis of an updated paleointensity database (Q PI-PINT) for 65-200 Ma: implications for the long-term history of dipole moment through the Mesozoic, *J. geophys. Res.,* 2018JB017287, doi:10.1029/2018JB017287.

Lawrence, K.P., Tauxe, L., Staudigel, H., Constable, C.G., Koppers, A., McIntosh, W. & Johnson, C.L., 2009. Paleomagnetic field properties at high southern latitude, *Geochem., Geophys. Geosyst.,* **10,** doi:10.1029/2008GC002072.

Lebedev, V.A., 2015. Geological map of Javakheti volcanic area (Lesser Caucasus), 1/200000, (2015), doi:10.13140/RG.2.1. 610 2359.2169.

Lebedev, V.A., Bubnov, S.N., Dudauri, O.Z. & Vashakidze, G.T., 2008. Geochronology of Pliocene volcanism in the Dzhavakheti Highland (the Lesser Caucasus). Part 1: western part of the Dzhavakheti Highland, *Stratigr. Geol. Correl.,* **16,** 204–224.

Lebedev, V.A., Chernyshev, I.V. & Sharkov, E.V., 2011. Geochronological scale and evolution of late Cenozoic magmatism within the Caucasian segment of the alpine belt, *Dokl. Earth Sci.,* **441,** 1656–1660.

Leonhardt, R., Heunemann, C. & Krasa, D., 2004. Analyzing absolute paleointensity determinations: Acceptance criteria and the software Thellier-Tool4.0, *Geochem., Geophys. Geosyst.,* **5,** 1–11.

Lund, S.P., 2018. A new view of long-term geomagnetic field secular variation, *Front. Earth Sci.,* **6,** 1–13.

Maisuradze, G.M. & Kuloshvili, S.I., 1999. Some geological problems of late volcanism in the dzhavakheti upland, *Tr. GIN AN Gruz. Nov. Ser.,* **114,** 220–228.

McElhinny, M.W. & McFadden, P.L., 1997. Palaeosecular variation over the past 5 Myr based on a new generalized database, *Geophys. J. Int.,* **131,** 240–252.

McElhinny, M.W., McFadden, P.L. & Merrill, R.T., 1996. The time-averaged paleomagnetic field 0–5 Ma, *J. Geophys. Res. Solid Earth,* **101,** 25007–25027.

McFadden, P.L. & McElhinny, M.W., 1982. Variations in the geomagnetic dipole 2: statistical analysis of VDMs for the past 5 million years, *J. Geomagn. Geoelectr.,* **34,** 163–189.

McFadden, P.L., Merrill, R.T. & McElhinny, M.W., 1988. Dipole/quadrupole family modeling of paleosecular variation, *J. geophys. Res.,* **93,** 11 583–11 588.

Merrill, R.T., McElhinny, M.W. & McFadden, P.L., 1996. *The Magnetic Field of the Earth. Paleomagnetism, the Core, and the Deep Mantle,* Vol. **63,** International Geophysics Series, Academic Perss.

Merrill, R.T. & Mcfadden, P.L., 2003. The geomagnetic axial dipole field assumption, *Phys. Earth planet. Inter.,* **139,** 171–185.

Nagata, T., 1963. Secular variation of the geomagnetic total force during the last 5000 years, *J. Geophys. Res.,* **68,** 5277–5281.

Paterson, G.A., 2011. A simple test for the presence of multidomain behaviour during paleointensity experiments, *J. geophys. Res.,* **116,** 1–12.

Paterson, G.A., 2013. The effects of anisotropic and non-linear thermoremanent magnetizations on Thellier-type paleointensity data, *Geophys. J. Int.,* **193,** 694–710.

Paterson, G.A., Biggin, A.J., Hodgson, E. & Hill, M.J., 2015. Thellier-type paleointensity data from multidomain specimens, *Phys. Earth planet. Inter.,* **245,** 117–133.

Paterson, G.A., Tauxe, L., Biggin, A.J., Shaar, R. & Jonestrask, L.C., 2014. On improving the selection of Thellier-type paleointensity data Greig, *Geochem., Geophys. Geosyst.,* **15,** 1180–1192.

Perrin, M. & Shcherbakov, V., 1997. Paleointensity of the Earth's magnetic field for the past 400 Ma: evidence for a dipole structure during the Mesozoic low, *J. Geomagn. Geoelectr.,* **49,** 601–614.

Prévot, M., Derder, M.E.-M., McWilliams, M. & Thompson, J., 1990. Intensity of the Earth's magnetic field: evidence for a Mesozoic dipole low, *Earth planet. Sci. Lett.,* **97,** 129–139.

Prévot, M., Mankinen, E.A., Coe, R.S. & Grommé, C.S., 1985a. The Steens Mountain (Oregon) geomagnetic polarity transition: 2. Field intensity variations and discussion of reversal models, *J. geophys. Res.,* **90,** 10 417–10 448.

Roberts, A.P., Tauxe, L., Heslop, D., Zhao, X. & Jiang, Z., 2018. A critical appraisal of the "day" diagram, *J. geophys. Res.,* **123**(4), 2618–2644.

Santos, C.N. & Tauxe, L., 2019. Investigating the accuracy, precision, and cooling rate dependence of laboratory-acquired thermal remanences during paleointensity experiments, *Geochem., Geophys. Geosyst.,* **20**(1), 383–397.

Selkin, P.A., Gee, J.S. & Tauxe, L., 2007. Nonlinear thermoremanence acquisition and implications for paleointensity data, *Earth planet. Sci. Lett.,* **256,** 81–89.

Shaar, R. & Tauxe, L., 2013. Thellier GUI: an integrated tool for analyzing paleointensity data from Thellier-type experiments, *Geochem., Geophys. Geosyst.,* **14,** 677–692.

Smirnov, A.V., Kulakov, E.V., Foucher, M.S. & Bristol, K.E., 2017. Intrinsic paleointensity bias and the long-term history of the geodynamo, *Sci. Adv.,* **3,** e1602306, doi:10.1126/sciadv.1602306.

Smirnov, A.V. & Tarduno, J.A., 2003. Magnetic hysteresis monitoring of Cretaceous submarine basaltic glass during Thellier paleointensity experiments: evidence for alteration and attendant low field bias, *Earth planet. Sci. Lett.,* **206,** 571–585.

Sánchez-Moreno, E.M., 2018. *Variation of the Absolute Paleointensity of the Earth's Magnetic Field Recorded in Sequences of Basaltic Flows from the Volcanic Region of Djavakheti (Georgia),* Universidad de Burgos, doi:10.13140/RG.2.2.30939.00804.

Sánchez-Moreno, E.M., Calvo-Rathert, M., Goguitchaichvili, A., Vashakidze, G.T. & Lebedev, V.A., 2018. Evidence of unusual geomagnetic regimes recorded in Plio-Pleistocene volcanic sequences from the Lesser Caucasus (Southern Georgia), *Geochem., Geophys. Geosyst.,* **19,** 1–18.

Tanaka, H. & Kobayashi, T., 2003. Paleomagnetism of the late Quaternary Ontake Volcano, Japan : directions, intensities, and excursions, *Earth, Planets Space,* **55,** 189–202.

Tanaka, H., Kono, M. & Kaneko, S., 1995. Paleosecular variation of direction and intensity from two pliocene-pleistocene lava sections in Southwestern Iceland, *J. Geomagn. Geoelectr.,* **47,** 89–102.

Tarduno, J.A., Cottrell, R.D., Davis, W.J., Nimmo, F. & Bono, R.K., 2015. A Hadean to Paleoarchean geodynamo recorded by single zircon crystals, *Science (80-),* **349,** 521–524.

Tauxe, L., 2006. Long-term trends in paleointensity: the contribution of DSDP/ODP submarine basaltic glass collections, *Phys. Earth planet. Inter.,* **156,** 223–241.

Tauxe, L., Gans, P. & Mankinen, E.A., 2004. Paleomagnetism and 40Ar/39Ar ages from volcanics extruded during the Matuyama and Brunhes Chrons near McMurdo Sound, Antarctica, *Geochem., Geophys. Geosyst.,* **5,** 1–20.

Tauxe, L., Gee, J.S., Steiner, M.B. & Staudigel, H., 2013. Paleointensity results from the Jurassic: new constraints from submarine basaltic glasses of ODP Site 801C, *Geochem., Geophys. Geosyst.,* **14,** 4718–4733.

Tauxe, L., Shaar , R., Jonestrask, L., Swanson-Hysell, N. L., Minnett, R., Koppers, A. A. P., *et al.*, 2016. PmagPy: software package for paleomagnetic data analysis and a bridge to the Magnetics Information Consortium (MagIC) Database, *Geochem., Geophys. Geosyst.,* **17,** 2450–2463, https://www2.earthref.org/MagIC, .

Tauxe, L. & Staudigel, H., 2004. Strength of the geomagnetic field in the cretaceous normal superchron: new data from submarine basaltic glass of the troodos ophiolite, *Geochem., Geophys. Geosyst.,* **5,** 223–241.

Thellier, E. & Thellier, O., 1959. Sur l'intensité du champ magnétique terrestre dans le passé historique et géologique, *Ann. Geophys,* **15,** 285–376.

Valet, J.-P., Meynadier, L. & Guyodo, Y., 2005. Geomagnetic dipole strength and reversal rate over the past two million years, *Nature,* **435,** 802–805.

Wang, H., Kent, D.V. & Rochette, P., 2015. Weaker axially dipolar time-averaged paleomagnetic field based on multidomain-corrected paleoin-tensities from Galapagos lavas, *Proc. Natl. Acad. Sci.,* **112,** 15 036–15 041.

Yamamoto, Y. & Tsunakawa, H., 2005. Geomagnetic field intensity during the last 5 Myr: LTD-DHT Shaw palaeointensities from volcanic rocks of the Society Islands, French Polynesia, *Geophys. J. Int.,* **162,** 79–114.

Yu, Y. & Tauxe, L., 2005. Testing the IZZI protocol of geomagnetic field intensity determination, *Geochem., Geophys. Geosyst.,* **6,** doi:10.1029/2004GC000840.

Yu, Y., Tauxe, L. & Genevey, A., 2004. Toward an optimal geomagnetic field intensity determination technique, *Geochem., Geophys. Geosyst.,* **5,** doi:10.1029/2003GC000630.

Zijderveld, J.D.A., 1967. A. C. demagnetization of rocks: analysis of results, *Dev. Solid Earth Geophys.,* **3,** 254–286.

SUPPORTING INFORMATION

Supplementary data are available at *GJI* online.

Figure S1. Schematic stratigraphic column of the Apnia sequence (location in Fig. 1). K-Ar datings from Lebedev *et al.* (2008). Polarity and Directional Groups (DG) are shown. The first image corresponds roughly to the lava flows of the upper section of the normal polarity sequence. The second ones are AP04 and AP14 flows, respectively. Modified after Sanchez-Moreno *et al.* (2018).

Figure S2. Normalized strong field magnetization versus temperature curves (Ms-T) of representative samples (modified after Sánchez-Moreno *et al.* 2018). The arrows indicate the heating and cooling curves. Curve types are discussed in the text.

Figure S3. Examples of hysteresis loops (corrected) and their corresponding IRM acquisition curves and back-field curves of samples from the Apnia sequence. These examples correspond to the same samples shown as types of thermomagnetic curves (M_S−T) examples in Fig. S2.

Figure S4. Bi-logarithmic Day-plot (Day *et al.* 1977) modified after (Dunlop 2002). M_{RS}/M_S: Saturation remanence to saturation magnetization. $B_{CR/BC}$: coercivity of remanence to coercivity.

Table S1. VADM calculated from the palaeointensities between 3 and 4 Ma (age covered by Apnia sequence) extracted from the PINT2015.05 database (Biggin *et al.* 2010).

Table S2. VADM calculated from the palaeointensities between 2.5 and 4.5 Ma extracted from the MagIC database (Tauxe *et al.* 2016) and interpreted by the RCRIT set of selection criteria.

Table S3. Palaeointensity results from (Calvo-Rathert *et al.* 2013) correlate with the results from this study by mean of palaeomagnetic information and directional groups obtained in (Sánchez-Moreno *et al.* 2018).

Please note: Oxford University Press is not responsible for the content or functionality of any supporting materials supplied by the authors. Any queries (other than missing material) should be directed to the corresponding author for the paper.